Microstructure of ultrathin films of $YBa_2Cu_3O_{7-\delta}$ on MgO

S. K. Streiffer, B. M. Lairson, C. B. Eom, B. M. Clemens, and J. C. Bravman
Department of Materials Science and Engineering, Stanford University, Stanford, California 94305

T. H. Geballe
Department of Applied Physics, Stanford University, Stanford, California 94305
(Received 20 November 1990; revised manuscript received 20 February 1991)

The microstructure of ultrathin films of $YBa_2Cu_3O_{7-\delta}$ on MgO has been studied for film thicknesses from 1.2 to 12 nm. For thicknesses of 1.2, 2.4, and 7.2 nm, the films appear to be in the tetragonal modification and consist of interconnected, low-aspect-ratio (thickness to diameter ratio ≤ 0.1) nuclei. The dominant growth mechanism is propagation in the a-b plane of one-unit-cell-high ledges by attachment onto the ledge face, resulting in a large difference between the c- and a-direction growth rates and forcing a two-dimensional appearance in the initial deposition. The 12-nm films are also tetragonal but provide complete coverage of the substrate. Their microstructure has passed the initial nucleation and growth stage and is similar to that of standard (thickness ≥ 100 nm) films. By analysis of the free energy of the tetragonal-to-orthorhombic transition occurring upon cooling from the deposition temperature, we note a film-thickness dependence of the energy available for the transition. We postulate this as an explanation for the lack of orthorhombicity in ultrathin films.

I. INTRODUCTION

It has been well demonstrated that the physical properties of $YBa_2Cu_3O_{7-\delta}$ are sensitive to the preparation conditions and resulting microstructure of this oxide material. In the case of thin films, many microstructural features are established in the initial moments of deposiston[1] when nucleation and growth first occur on the bare substrate; therefore, an understanding of nucleation and growth may allow better control of the film's final microstructure and thus its properties. One method for exploring this area is by examining ultrathin films, in which deposition has been halted after only a very brief time, such that the initial coverage of a small number of unit cells can be directly observed. In addition, ultrathin films are themselves of interest as a model system to study the fundamental properties and possibly reduced dimensionality of the superconducting state in $YBa_2Cu_3O_{7-\delta}$ and as a reference for investigations of multilayer structures incorporating such thin $YBa_2Cu_3O_{7-\delta}$ regions. To fully understand the implications of measurements made on ultrathin films and to draw conclusions on ways to control the growth and microstructure of standard films, a detailed and comprehensive understanding of the microstructure and crystallography of the ultrathin system is essential. By way of introduction we will briefly describe known properties of ultrathin films and then use this as a starting point for defining our detailed investigation of the microstructure and morphology of these films.

A. Previous studies

Several groups[1-13] have reported on the properties of ultrathin $YBa_2Cu_3O_{7-\delta}$ films grown on a variety of annealed[1-4] and unannealed[5-7] substrates by a number of techniques, including laser ablation, reactive evaporation, and sputtering. In general, it is found that the superconducting transition temperature begins to fall and that the resistive transition width begins to increase below a thickness of about 10 nm, with best case T_{c0}'s reported for 3-nm films lying around 45 K, with ΔT_c's of approximately 25 K;[2,7,12] in one case Michikami, Asahi, and Asano report a T_c of 25 K for a 2-nm film.[3] X-ray diffraction, reflection high-energy electron-diffraction (RHEED), and Rutherford-backscattering spectrometry (RBS) studies indicate that the $YBa_2Cu_3O_{7-\delta}$ c axis is normal to the substrate, that there is strong in-plane texture even in these very thin films, and that crystal quality is somewhat degraded.[2,6,10] Most groups observe $[100]_{film}\|[100]_{substrate}$, although the $[110]_{film}\|[100]_{substrate}$ orientation relationship was observed for EuBCO films deposited on MgO by planar magnetron sputtering.[3]

Since crystal structure is strongly correlated with other properties of $YBa_2Cu_3O_{7-\delta}$ such as T_c,[13] it is important to distinguish between effects due to changes in the crystallography of ultrathin films and changes in properties due to other factors. With this in mind, two elements of the crystal structure must be considered: the symmetry of the lattice, i.e., tetragonal or orthorhombic, and the absolute value of the in-plane lattice parameter, since below a certain critical thickness h_c the film will be strained elastically to match the substrate-lattice parameter.[14] It appears that for these thicknesses $YBa_2Cu_3O_{7-\delta}$ exhibits its tetragonal modification even under oxidation conditions that should allow the film to become orthorhombic.[8,12] No conclusive data exists on the precise thickness at which orthorhombicity first occurs, and it can be expected to depend on substrate and deposition

conditions: there are conflicting results on the symmetry of 10-nm films on MgO.[10,12] Second, ultrathin $YBa_2Cu_3O_{7-\delta}$ is below h_c and thus strained toward the substrate-lattice parameter ($a=0.39$ nm) in the case of $YBa_2Cu_3O_{7-\delta}$ on $SrTiO_3$,[8] while on MgO substrates even single-unit-cell films show the "bulk," average tetragonal a-axis length of 0.385 nm.[9]

The growth mode and morphology of ultrathin $YBa_2Cu_3O_{7-\delta}$ has been studied primarily by two sets of investigators. Bando and co-workers, using RHEED, inferred that growth appears to be layer by layer in their deposition system (activated reactive evaporation),[9,12] and that on $SrTiO_3$ half-order streaks in the RHEED pattern indicate that local oxygen ordering into Cu-O chains might exist.[8] Norton *et al.*[1,4] have used transmission electron microscopy (TEM) to examine films laser ablated onto prethinned, acid-cleaned, and then annealed MgO substrates. In contrast to the above results, they determined that their films consist of large interconnected islands and that the coalescence of these often rotationally misaligned ($\sim 1°$ or 2°) islands leads to the formation of dislocations and incipient voids. From an estimate of the volume of material ablated, a film covering 50% of the substrate was shown to have interconnected islands approximately 12 nm thick and 20 nm in lateral extent. They propose that film alignment with MgO⟨100⟩ surface steps, a graphoepitaxial process, increases the perfection of the macroscopic orientation relationship and increases film quality.

B. Questions addressed by current work

Several issues remain to be fully explored. First, as discussed in the preceding paragraph, different growth modes (two-dimensional layer-by-layer growth versus three-dimensional island growth) have been reported for different deposition techniques; factors relating to competition between the two have yet to be elucidated. Most applications of ultrathin $YBa_2Cu_3O_{7-\delta}$ require it to be as uniform as possible, making two-dimensional growth the preferred mode. In order to explore the issue of growth dimensionality, we have used TEM to investigate a systematic through-thickness series of ultrathin $YBa_2Cu_3O_{7-\delta}$ films on MgO. Besides facilitating this type of study, it allows us to track the development of film microstructure from the initial nucleation and growth stage to the point at which bulk thin-film microstructure is achieved. With such information one can better interpret physical properties measurements taken at particular stages of film thickness and controllably manipulate nucleation and growth to obtain different film characteristics.

Second, although there exists a treatment of the tetragonal-to-orthorhombic transformation for thin films rigidly constrained at the substrate (elastic deformation in the film due to the transformation),[15] we will justify and develop a free-energy analysis of the transformation in which a $YBa_2Cu_3O_{7-\delta}$ film is allowed to move plastically with respect to the substrate. From this theoretical framework we develop a model which is consistent with the lack of orthorhombic symmetry in such extremely thin deposits of $YBa_2Cu_3O_{7-\delta}$. An understanding of this behavior is important for the actual application of ultrathin films since it has implications for the "achievable" crystal structure of the $YBa_2Cu_3O_{7-\delta}$.

Finally, implications of the above investigations for the microstructure of multilayer films will be discussed. As in the bare ultrathin system, a clear understanding of the microstructure is essential to define rigorously the experimental configuration probed in a particular measurement.

II. EXPERIMENTAL PROCEDURES

The ultrathin films examined in this work were grown on MgO substrates by single-target, off-axis magnetron sputtering. Details of the deposition process have been reported elsewhere;[13,16] only a brief description is presented here. To begin, optically polished MgO substrates were cleaned in organic solvents. Since the initial thrust of this work was to examine factors influencing the microstructure of our standard, high-quality, thicker (≥ 100-nm) films which are deposited on unannealed substrates, the substrates used in this study were also unannealed. These were next attached with silver paste to the substrate block in our deposition chamber, which is positioned at 90° to the sputtering target to avoid preferential resputtering of the film by negative ions and a concomitant loss of stoichiometry.[13] The sputtering was performed from a stoichiometric $YBa_2Cu_3O_{7-\delta}$ target in 10 mtorr oxygen and 40 mtorr argon with a rf power of 125 w, at a block temperature of 650–670 °C. After deposition the chamber was vented to 500 torr oxygen and allowed to cool to 100 °C. At this point the chamber was reevacuated, and because of the susceptibility of $YBa_2Cu_3O_{7-\delta}$ to environmental degradation and oxygen loss, a protective overlayer of amorphous $YBa_2Cu_3O_{7-\delta}$ was deposited on the just-grown films, a technique originally described by Xi *et al.*[2] Because of this overlayer, reliable electrical contact could not be made to the underlying films for resistive T_c determination, but similar 3-nm ultrathin films deposited in our system without the overlayer demonstrated T_c's of 45 K.[7,13] Any persistent current at 4.2 K was below the sensitivity of our vibrating-sample magnetometer ($\sim 10^{-3}$ emu or $\sim 10^5$ A/cm^2 for a 10-nm-thick, 6×6 mm^2 sample) for all the specimens discussed here.

Four nominal film thicknesses were investigated: 1.2, 2.4, 7.2, and 12 nm; these numbers correspond to extrapolations from deposition rates for thicker films and serve as rough guides only, as will be apparent later. A brief description of some of these samples has been presented elsewhere.[17] Samples of the same 6×6 mm^2 specimen were prepared for both plan-view and cross-sectional microscopy using standard techniques. Care was taken to avoid contact of the specimen with water at all times, and the samples were ion milled at reduced voltages (4 kV) and currents (0.3 mA) and cooled by a cold finger immersed in liquid nitrogen to avoid damage to the films. Viewing was performed in a Philips 430ST at 300 kV

along one of the ⟨001⟩ zone axis of the MgO substrates. The micrographs shown here are all multibeam zone-axis images. In addition, to further characterize the microstructure of these ultrathin films, the 2.4-nm film was examined by grazing-incidence x-ray scattering (GIXS) at the Stanford Synchrotron Radiation Laboratory on beam line 7-2, using a wavelength of 0.15091 nm and a constant reciprocal space l component of the grazing-incidence scans of 0.1841 nm^{-1}. Finally, the 12-nm sample and one 300-nm-thick reference sample were examined by GIXS to investigate the orthorhombicity of ultrathin film $YBa_2Cu_3O_{7-\delta}$, using a four-circle diffractometer with a rotating anode Cu $K\alpha$ source operated with a large beam divergence to ensure sampling of the entire thickness of the film.

III. RESULTS AND DISCUSSION

A. Through-thickness investigation

Low-magnification examination of all samples showed them to consist exclusively of the $YBa_2Cu_3O_{7-\delta}$ film and MgO substrate. Selected-area diffraction (Fig. 1) revealed that all samples were c-axis oriented with no a-axis material present and that all spots in the electron-diffraction patterns could be indexed to a single $YBa_2Cu_3O_{7-\delta}$ in-plane lattice parameter of approximately 0.385 nm, the MgO, or to double diffraction between these two materials. For no ultrathin-film thicknesses did we observe splitting of the $YBa_2Cu_3O_{7-\delta}$ diffraction spots or any extra periodicities in the diffraction pattern. This strongly suggests that the films are tetragonal with regard to unit-cell axial lengths. All four thicknesses exhibited the orientation relationship $[100]_{YBa_2Cu_3O_{7-\delta}} \| [100]_{MgO}$. In addition, a small amount of material rotated 45° in the plane was found in the 2.4-nm sample.

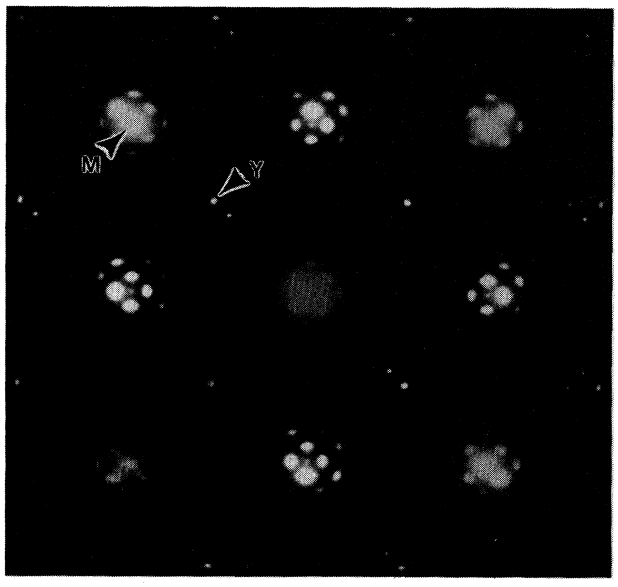

FIG. 1. Plan-view electron-diffraction pattern of 2.4-nm-thick $YBa_2Cu_3O_{7-\delta}$ film on MgO. The $YBa_2Cu_3O_{7-\delta}$ (100) spot is indicated by Y and the MgO (200) by M for reference. The spot intensities in this pattern have been substantially altered such that the $YBa_2Cu_3O_{7-\delta}$ spots are visible on the final photograph.

To further explore the question of the in-plane symmetry of the 12-nm film, GIXS was used to scan the region in reciprocal space about the $YBa_2Cu_3O_{7-\delta}$ (200) and (220) peaks. Only single peaks were found at the tetragonal reciprocal space locations. From analysis of the (220) and (200) peak breadths and from an analysis of the minimum detectable orthorhombic splitting for these reflections, we place an upper bound of 0.0013 nm on any possible difference in unit-cell axial lengths, compared to 0.0066 nm for the fully orthorhombic structure. This, taken with the electron-diffraction data and the evidence in the literature,[8,12] leads us to conclude that all of the ultrathin films studied here are tetragonal or, at the very least, of greatly reduced orthorhombicity.

For the 2.4-nm film, the GIXS data are also entirely consistent with a tetragonal structure. A value of 0.3850 nm was found for the $[100]_{MgO}$-aligned in-plane lattice parameter, with a slight asymmetric broadening of the diffraction peak toward smaller d spacings. The mosaic spread of the in-plane orientation, as measured by the full width half maximum of the film (200) peak upon rotation of the sample about the surface normal of the substrate, was 1°. The in-plane coherence length as deduced by the Scherrer formula was 30 nm. This peak breadth limits our sensitivity to an upper bound of 0.002 nm for any possible difference in unit-cell axial lengths. For this particular specimen the ratio of the intensity of the peak from 45° rotated material to that of the peak from [100]-aligned material was 0.013. In addition, the a-axis lattice parameter measured for the 45° material was 0.3841 nm, slightly smaller than that of the [100]-aligned portion of the film, although the in-plane mosaic spread and Scherrer coherence length for this orientation of the film were the same as for the [100]-aligned $YBa_2Cu_3O_{7-\delta}$.

Figure 2 shows the plan-view image of the 1.2-nm film, which is seen to consist of impinging nuclei generally a few tens of nanometers in size. This micrograph, as well as all other micrographs in this work, are multibeam zone-axis images formed on the $YBa_2Cu_3O_{7-\delta}$ [001] zone axis for plan views or the $YBa_2Cu_3O_{7-\delta}$ [100] zone axis for cross sections. The moiré fringe contrast in the image arises from the difference of the MgO and $YBa_2Cu_3O_{7-\delta}$ (200) interplanar spacings, giving a fringe spacing of 2.3 nm, neglecting rotational misalignment effects on the moiré pattern. As an aside, orthorhombicity of the $YBa_2Cu_3O_{7-\delta}$ would manifest itself as a spacing difference in orthogonal moiré fringes. In practice, rotational effects and the large moiré fringe spacing limit sensitivity to orthorhombicity, especially over small length scales. Still, no systematic spacing difference in orthogonal moiré fringes was measured for any of the films studied here, thus not voiding the conclusion of tetragonality of the films. For discrete unit cells on a thick, high-quality, single-crystal substrate, as is the case here, these

fringes represent reasonably faithfully a magnification of the lattice of the film rather than that of the substrate. This conclusion, and film-thickness effects on the image, are discussed below. The darker mottling is electron-beam-induced damage of the MgO substrate. At this stage of deposition, the film consists of interconnected nuclei a few tens of nanometers in size, with a microstructure only qualitatively similar to that observed by Norton *et al.*[1,4] in laser-ablated films. Cross sections confirm that areas between moiré islands are indeed bare within the resolution of one or two atomic layers (determination of mono- or bilayer coverage is made impossible here by the continuous amorphous overlayer) and that even single-unit-cell $YBa_2Cu_3O_{7-\delta}$ layers have an in-plane lattice constant clearly relaxed from that of MgO. Overall coverage estimated from the moiré patterns for this deposited volume is about 25%—in the region of Fig. 2 it is higher, but there seems to be a tendence for nuclei to cluster nonuniformly such that there are equally large regions of substrate that are totally bare.

As demonstrated by Dahmen, Hetherington, and Westmacott,[18] and Hetherington,[19] moiré fringes can be used as a magnifier of inhomogeneous strain. Clearly, the initial deposit contains significant plastic and elastic strain as evidenced by the frequent curving of the fringes. At the intersection of these often rotationally misaligned nuclei ($< 1.5°$), a variety of defects are apparent. Both full, two terminating (200) moiré fringe (marked *d*) and partial, one terminating (200) moiré fringe (marked *p*) dislocations are observed, with full, two fringe dislocations much more common. These dislocations could arise both from the rotational misalignments and from the intersection of nuclei originating a nonintegral number of $YBa_2Cu_3O_{7-\delta}$ unit cells away from each other. An $a/2$ translation boundary or antiphase boundary is marked by the arrow. Since the interisland rotations involved here are small, it is likely that this boundary is not an equilibrium structure and should relax into dislocations in an unfaulted lattice, as seen elsewhere in this film. Preferential faceting of the nuclei is observed along {100} planes, and to a lesser extent along {110} planes, on a length scale of tens nanometers, similar to the structure seen by Norton *et al.*[1,4] Since the image is a projection of the true structure, the observed faceting corresponds to faceting only of the leading edges of the nuclei. The leading edge in this context is the farthest extending growth front, which is the first layer directly on the substrate, plus any higher layers sharing the same end point as the first, since there is no overhang.

Cross-section micrographs show that the initial deposi-

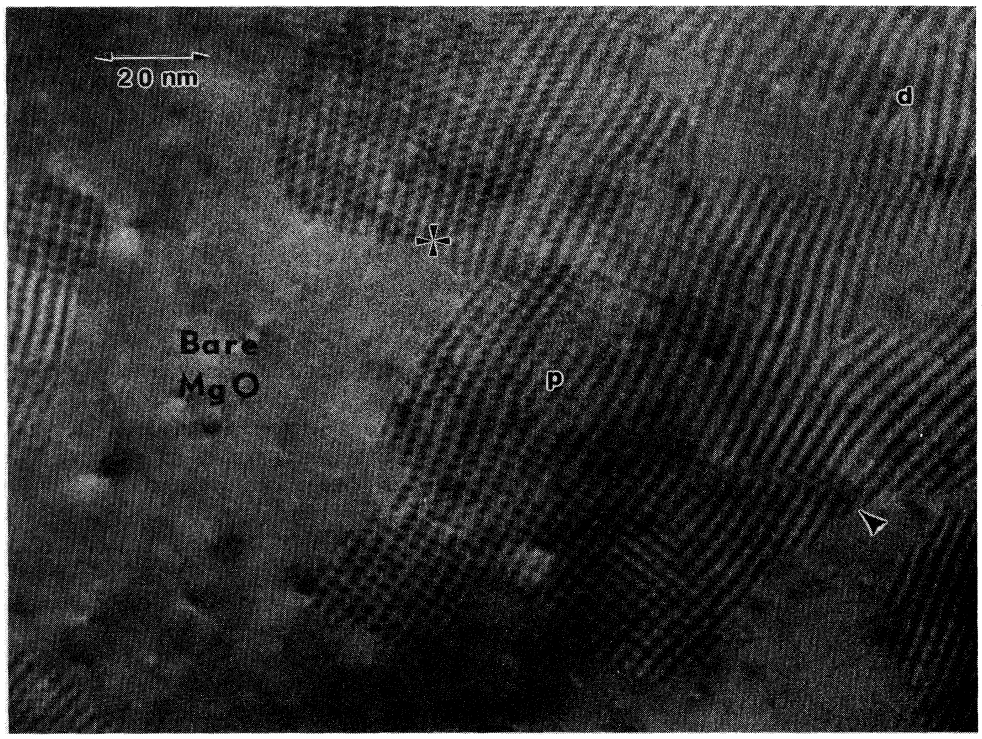

FIG. 2. Plan-view image of 1.2-nm-thick film showing moiré fringes arising from spacing difference of $YBa_2Cu_3O_{7-\delta}$ and MgO (200)'s. Fringe spacing is approximately 2.3 nm. Dark and light background mottling is due to electron-beam-induced damage in the MgO substrate. A variety of defects are present, including full dislocations, example marked *d*, partial dislocations, example marked *p*, and a translation boundary, marked by the arrow. Also present are abrupt integrated image intensity changes due to discrete thickness changes in the film. The end of one such boundary is marked by a star.

tion produces nuclei that are one, two, and, infrequently, three unit cells high. Because of projection effects, however, the spatial distributions of these various nuclei thicknesses are difficult to determine by such cross-sectional examination. Instead, we note in Fig. 2 that in this plan-view image there are discrete contrast variations in and between the islands; an end of a boundary between two such regions is marked with a star. By calculation of the Pendelløssung plots for the various diffracted beams of $YBa_2Cu_3O_{7-\delta}$ (using MacTempas simulation software[20]) and assuming that the MgO is on the order of tens of nanometers thick and reasonably uniform over the dimensions of a $YBa_2Cu_3O_{7-\delta}$ island, it is evident that these abrupt intensity changes are due to changes in the number of $YBa_2Cu_3O_{7-\delta}$ unit cells on the substrate. The assumptions concerning MgO are known to be fulfilled because imaging is done in thicker regions well away from the edge of the ion-milling perforation and because cross-sectional microscopy and atomic force microscopy[13] show that the surface roughness of MgO after exposure to deposition conditions is about 3 nm over a lateral distance of tens of nanometers. The ion-milled sample back side is expected to have similar roughness. These small percentage variations in the MgO assure us that it contributes minimally to the observed rapid contrast variations. In addition, viewing away from the perforation ensures that the moiré fringes are not lost because of the milling away of MgO, but not the milling away of the $YBa_2Cu_3O_{7-\delta}$ or the amorphous overlayer. Dislocations in the MgO are quite visible and distinctive in conventional microscopy, and areas containing them are also avoided. Thus the MgO substrate acts only as a reference lattice in the fashion of the artificial lattice used by the Berkeley researchers[18,19] and not as a contrast source, except for electron-beam damage.

The Pendelløssung plots for $YBa_2Cu_3O_{7-\delta}$ of up to 4.8 nm are shown in Fig. 3. For one, two, and three unit cells, the (110) diffracted beam behaves almost kinematically, with only a small phase change. Thus an abrupt intensity change has an easily interpreted one-to-one correspondence with a change in thickness, which because of its magnitude must be a single-unit-cell increment, over a distance equal to or less than the resolution of the moiré pattern of 1.2–2.4 nm. From cross-section data discussed below, we know that the unit-cell-thickness changes are actually almost atomically abrupt. Extending this analysis, dark-field imaging with the (110) beam in plan view yields a situation where three-dimensional information is available from one imaging direction. By careful analysis of the image intensity, we are able to extract the two-dimensional morphology of the different layer thicknesses. Preliminary work indicates that this approach is indeed feasible and that faceting of the upper $YBa_2Cu_3O_{7-\delta}$ layers is on a much smaller length scale, on the order of a few nanometers, than of the $YBa_2Cu_3O_{7-\delta}$ layer directly on the substrate. However, because of the long film exposure times necessary and the resulting specimen drift, the analysis is not as straightforward as might be desired; therefore, the body of these investigations will be reported elsewhere.

Figure 4(a) shows a plan-view micrograph from the

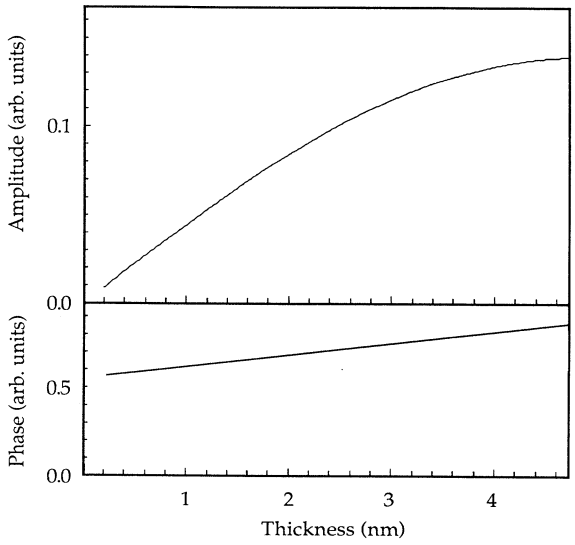

FIG. 3. Pendelløssung plots of the $YBa_2Cu_3O_{7-\delta}$ (110) diffracted beam for $YBa_2Cu_3O_{7-\delta}$ thicknesses up to 4.8 nm. Note that for these thicknesses, the amplitude increases monotonically with thickness and the phase changes slowly, allowing thickness discrimination by image intensity.

2.4-nm sample. The film still consists of interconnected islands of size 20–50 nm, and a general survey of the sample shows that coverage is now more uniform and has doubled to about 50%. Figure 4(b) is a cross section of this sample: proper *c*-axis direction structure and an incoherent film-substrate interface are visible. The film thickness is still consistently two unit cells at this stage; in addition, the amorphous $YBa_2Cu_3O_{7-\delta}$ overlayer is visible. Relative to the 1.2-nm film, we have not increased the thickness, but rather increased coverage with approximately the same island thickness. This behavior may be understood in the following manner. Figure 4(c) illustrates the transition region from a thickness of two unit cells to one unit cell. It is apparent that the relevant mechanism for growth is propagation of unit-cell-high ledges in the $YBa_2Cu_3O_{7-\delta}$ *a-b* plane, as marked by the arrow. This ledge structure allows parallel attachment of all elements, as opposed to growth purely in the *c*-axis direction where single-element layers must be sequentially formed. Since the films are deposited by a single-target technique, producing all species simultaneously, the former growth mode should be preferred. Thickness changes not involving such a unit-cell step have not been observed; nor have unit-cell steps with different *c*-axis layering sequences been found. After the initial nucleation event which produces the one-, two-, and three-unit-cell islands, the incoming flux is mostly consumed by propagation of these unit-cell ledges. Once coverage is such that the incident flux can no longer be consumed by the existing layers, the film will macroscopically thicken. The height of the nuclei may be controlled by the initial roughness of the MgO substrate, which could act to reduce the lateral propagation of the nuclei (and thus the

anisotropy of *c* axis to *a-b* plane growth) until they are higher than this incipient surface roughness. Furthermore, it could be that MgO surface roughness acts as a source of heterogeneous nucleation sites, also, in effect, controlling nuclei heights. These growth-mode observations are consistent with the RHEED observations of Bando *et al.*,[12] but contrary to the film microstructure observed by Norton *et al.* in which islands were much larger and thicker.[4]

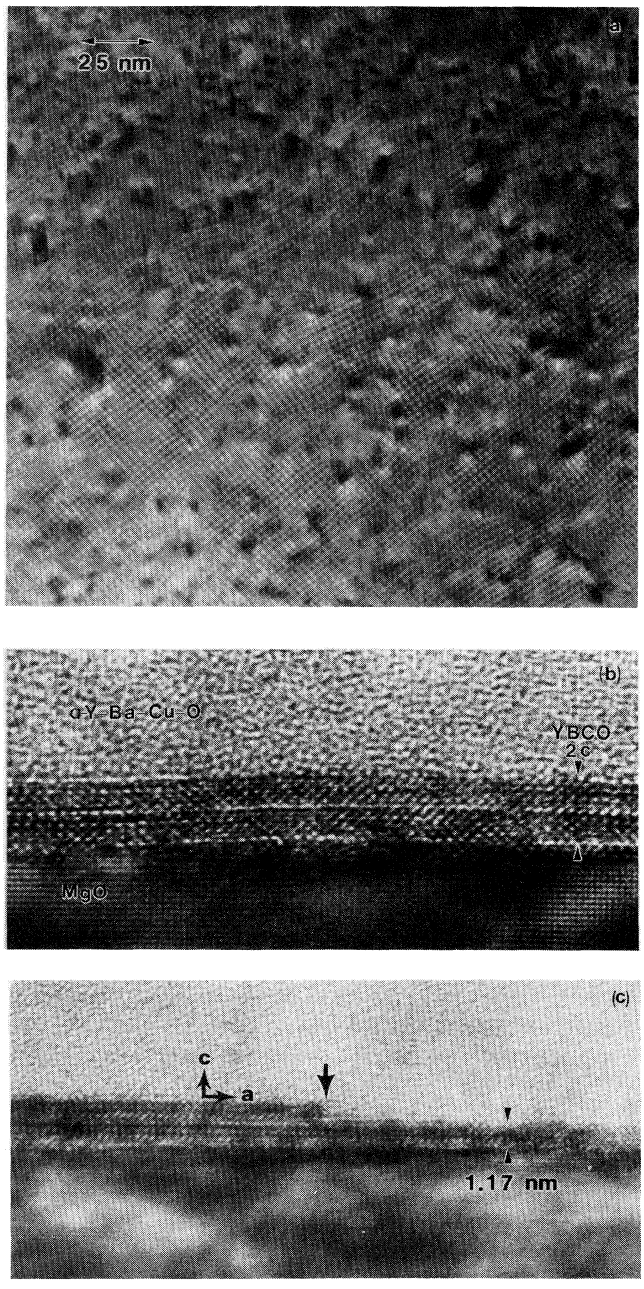

FIG. 4. (a) Plan-view image of 2.4-nm film. Note increased substrate coverage over 1.2-nm film. (b) Cross section of 2.4-nm film. Visible are the MgO, the two-unit-cell-thick $YBa_2Cu_3O_{7-\delta}$ film, and the amorphous $YBa_2Cu_3O_{7-\delta}$ (α-Y-Ba-Cu-O) overlayer. Note the frequent curving of the lattice planes in the $YBa_2Cu_3O_{7-\delta}$ film. (c) Cross section showing unit-cell-high ledge, marked by large arrow. The $YBa_2Cu_3O_{7-\delta}$ crystallographic directions are as indicated.

Thus the growth of these films occurs in a two-dimensional, layer-by-layer fashion, where the ledge is a complete *c*-axis unit and propagates in the $YBa_2Cu_3O_{7-\delta}$ *a-b* plane. The "island" morphology seen in plan-view images here is then due to a large number of nucleation sites rather than true three-dimensional islanding. Several factors probably conspire to produce this behavior. First, the rough surface of MgO, as discussed earlier, should provide the requisite large number of initial nucleation sites. Second, the intrinsic anisotropy of the $YBa_2Cu_3O_{7-\delta}$ crystal structure imposes a preferential growth direction, for the reasons of parallel attachment mentioned in the preceding paragraph. Third, close examination of Fig. 4(a) and 4(b) shows that there seems to be preferential stable termination of the $YBa_2Cu_3O_{7-\delta}$ surface by a particular elemental species or a preferred stable ionic unit, as evidenced by similar contrast everywhere at the top surface and also by the constant stacking structure of the unit-cell-high ledges. Based on the crystallographic position of the terminating layer and using image contrast as a suggestive guide, we believe the terminating metal species to be Ba, although occasionally it appears to be Cu. Some uncertainty in this observation is induced by the amorphous overlayer. Schlom[21] has investigated with RHEED a similar phenomenon in the Bi-Sr-Ca-Cu-O system, where only a particular structural unit of the superconducting phase was found to be stable as that phase, for their shuttered molecular-beam-epitaxy deposition conditions. Finally, preferential stable termination of the MgO surface by a particular $YBa_2Cu_3O_{7-\delta}$ crystallographic layer[22] may also help to establish a specific ledge structure for the layer directly on the substrate. Given this ledge structure, whether or not single atomic layer growth can be achieved thus seems a question best addressed by elementally sequential techniques such as shuttered molecular-beam epitaxy, although as implied above it has yet to be achieved. The transition from layer-by-layer growth to large island growth is likely controlled by factors moving the macroscopic *a-c* growth-rate ratio more toward unity. These factors could include very large surface roughness on the substrate producing very thick nuclei, high instantaneous growth rates as might occur in laser ablation, and a high nucleation rate for new layers on top of old ones.

Figure 5(a) is a plan-view micrograph of a nominally 7.2-nm-thick film. At this thickness the film is almost continuous; overall coverage is estimated to be $>80\%$. With this great a coverage, we can measure the incipient threading dislocation density produced by island impingement: for this film it is approximately 10^{11} cm/cm^3. For comparison, the dislocation density in heavily cold-worked metal is in the neighborhood of 10^{12} cm/cm^3.[23] This density of dislocations corresponds to an interdislocation spacing of about 35 nm with each dislocation running through the thickness of the film.

Cross-section studies show that the film thickness is six unit cells as targeted, but still varies by two unit cells.

That this is the same roughness as in the two thinner films reinforces our conclusions on the microscopic thickening mechanism and the two-dimensional nature of growth. Figure 5(b) demonstrates the robustness of the *c*-axis layered growth in this material—continuity is often maintained even over large surface perturbations. By the introduction of low-angle boundaries (marked with arrows), the film is able to continue its growth right over the surface outcropping in this image. This must occur by attachment to the existing $YBa_2Cu_3O_{7-\delta}$ much like growth onto a seed crystal from a melt, rather than by epitaxial mechanisms influenced by the substrate. This emphasizes an important feature of $YBa_2Cu_3O_{7-\delta}$ deposited on MgO: even though the initial nuclei are highly oriented with respect to the substrate, because of a variety of possible factors including graphoepitaxy,[4] epitaxy of a precursor species saturating the substrate surface, or near-coincident site lattice effects,[24] continuation of coverage of the MgO is an attachment process that is not strictly epitaxial in nature. In addition, because of this tolerance of surface roughness, the $YBa_2Cu_3O_{7-\delta}$ film near the substrate is substantially strained not only in the plane of the substrate surface as seen in the above plan-view moiré images, but also normal to the surface, as is apparent in the cross sections presented here and by other workers.[6,25]

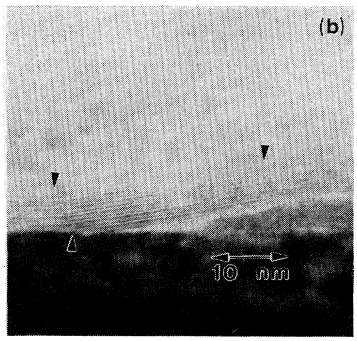

FIG. 5. (a) Plan-view micrograph of the 7.2-nm film. At this stage coverage is nearly complete. The threading dislocation density measured from this image is 10^{11} cm/cm^3. A representative dislocation lies between the arrows; viewing is best performed by sighting down the moiré fringes. (b) Cross section of 7.2-nm film. The film has grown over a substrate surface perturbation, with the strain partly accommodated by low-angle boundaries, marked by arrows. There is some ion-mill damage of the film in this region, increasing toward the right of the image.

Examination of the 12-nm film (Fig. 6) reveals that at this stage coverage is complete and that the microstructure is beginning to resemble that of thicker films, although it is still somewhat granular in nature. At this thickness, deposition has clearly moved past the initial film-substrate nucleation phase. For greater thicknesses we would expect the effective grain size to coarsen by classical mechanisms and for some of the strain in the layers to relax, as has been inferred from microscopy of standard films by the workers at Bellcore and Rutgers.[6,25]

The observation of granularity even at 12 nm is interesting in light of the interpretation of the superconducting transition of a 20-nm $YBa_2Cu_3O_{7-\delta}$ film on $SrTiO_3$ in terms of percolative behavior and granularity by Leemann *et al.*[26] They assume the grain size of their 20-nm-thick sample to be around 1 μm and thus deduce that percolation in their system is two dimensional; this is inconsistent with our domain-size observations, albeit that our observations are of films on MgO. We emphasize the importance of a detailed description of films in this thickness regime when interpreting physical properties influenced by microstructure.

One final point concerning the thickness of the four films discussed here should be noted. The thinnest two films contain a smaller volume of material than inferred from the deposition rate calculated from the sputtering of thicker films. This can be attributed to two factors. First, there is a short time period necessary to establish steady-state deposition conditions. Second, nucleation on the substrate may be difficult and thus it may require some short interval to achieve a steady growth rate. The

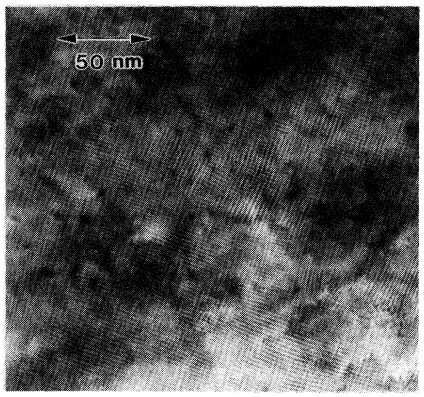

FIG. 6. Plan-view image of the 12-nm film.

deposition times for the 1.2- and 2.4-nm films were on the order of 1–2 min, a short enough period such that these transient phenomena are still evident. For the 7.2- and 12-nm films, the actual thickness agrees with that calculated from the deposition rate; for these two the transient period is negligible relative to the total deposition time.

B. Tetragonal-to-orthorhombic transition

It is well known that upon cooling in oxygen $YBa_2Cu_3O_{7-\delta}$ transforms from a tetragonal to an orthorhombic state. Contrary to this behavior, ultrathin films remain in what appears to be the tetragonal state. If we restrict our attention to the case of $YBa_2Cu_3O_{7-\delta}$ on MgO with approximately parallel [100]'s, where no lattice-matching strain is present even for single unit cells, then a free-energy expression can be written for the phase transition building on the work of Arlt, Hennings, and de With,[27] Welch,[28] Roitburd,[15] and Lairson, Streiffer, and Bravman.[29] Based on the microstructural data discussed above, the thickness at which films cease to become orthorhombic (around 10 nm) is on the high-coverage tail of the crossover region from island coverage to uniform coverage for our films; with this in mind two regimes for the transition with different free-energy expressions are relevant: (I) the case where the film is completely connected and uniform as in the standard thin film case, and (II) the case where the film consists of unconnected islands that are free to change shape independently. The case most appropriate for our circumstances is the first, but the analysis for both is included here for completeness.

Starting with case I and noting that this transformation would be accommodated by twinning, the free-energy per unit volume, Δg, can be approximated as a sum of terms:

$$\Delta g = \Delta g_{\rm th} + \Delta g_{\gamma} + \Delta g_{m} + \Delta g_{I} \ , \tag{1a}$$

where $\Delta g_{\rm th}$ is the thermodynamic free energy of the tetragonal-to-orthorhombic transition, Δg_{γ} is the twin-boundary interfacial free energy, Δg_{m} is the elastic energy due to a finite twin-domain size imposing a geometric constraint on the transition, and Δg_{I} is the energy required to deform the film elastically[15] or plastically with respect to the substrate. The first three terms are a result of the phase transition in $YBa_2Cu_3O_{7-\delta}$ only and are shared by both bulk and thin-film systems; the last is particular to a thin film on a rigid substrate and, as will be shown below, is the source of the observed thickness behavior of the orthorhombicity.

If the twinning transformation occurred elastically such that the film was rigidly attached to the substrate at the interface while the upper regions became more orthorhombic with increasing distance from the substrate, then to a first approximation this could be modeled as an average lattice parameter plus an inhomogeneous strain term. This is inconsistent with available x-ray- and electron-diffraction data,[30,31] which are attributable to a homogeneous and fully split orthorhombic structure. An example of this splitting in a 300-nm film is shown in Fig. 7. This GIXS scan of the {110} peaks upon rotation of the sample about the surface normal of the substrate shows three clear peaks, which were fit by Pearson VII functions to obtain widths and positions. For a detailed description of the twin structure and resulting x-ray-diffraction patterns, readers are referred to Budai, Feenstra, and Boatner,[30] Barry,[32] and Schmid *et al.*[33] Briefly, four sets of twin domains are sampled by the x rays. This leads to a strong central peak aligned exactly with the substrate [110] with two side peaks of about one-half the central peak's intensity. The central peak is due to the two sets of domains whose twin boundary is normal to the scattering vector q; the two side peaks are from the orthogonally oriented twin domains and are angularly split from the central peak as a result of the shear caused by the twinning. The intensity difference is easily explained as arising from the fact that the (110) aligned with the twin boundary has a coherently scattering material volume twice that of the (110) crossing the twin boundary, because the noncrossing (110) is the same on both sides of the twin boundary, while the crossing (110) is sheared and is not the same across the boundary. Peak splitting in Fig. 7, 1.8° between the two side peaks, is precisely that predicted by geometrical considerations of twinning in a homogeneously transformed volume and is completely consistent with the observed angular and reciprocal space splittings of the {200} and {020} peaks. Peak broadening in θ-2θ in these patterns is also entirely consistent with the twin spacings measured by TEM. Finally, the elastic model predicts a $t^{1/3}$ film-thickness dependence of the twin spacing; the observed dependence in our films is more consistent with $t^{1/2}$.[29] Given that $YBa_2Cu_3O_{7-\delta}$ is not lattice matched to MgO for any

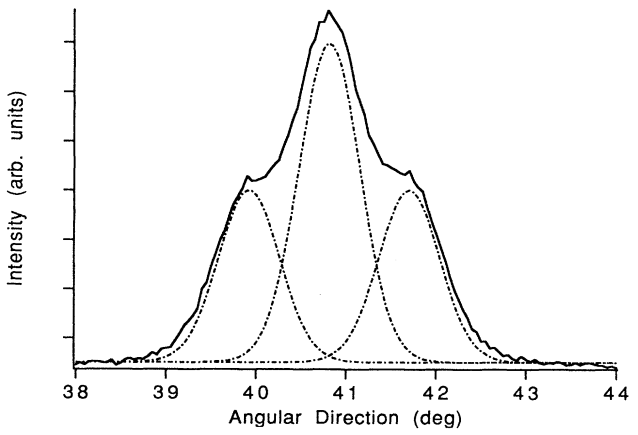

FIG. 7. Glancing-incidence x-ray-scattering spectrum upon rotation about the surface normal of a 300-nm-thick $YBa_2Cu_3O_{7-\delta}$ film on MgO. The pattern consists of three $YBa_2Cu_3O_{7-\delta}$ {110} peaks split due to twinning. Peaks from a least-squares fit to three Pearson VII functions are shown with dotted lines. Note that the zero point of the rotation is such that the MgO [100] direction lies at −4.2°.

thickness and that the film-substrate interface is incoherent as shown above, it is not surprising that the interface is not locked and rigid.

Therefore, assuming that film deformation occurs plastically, we can write Eq. (1a) explicitly as

$$\Delta g = \Delta g_{\rm th} + \frac{\gamma}{l} + \frac{clMs^2}{h} + \frac{\sigma_c sl}{4t} , \tag{1b}$$

where γ is the twin-boundary energy, l is the twin spacing, $s=(b/a)-1$ is the orthorhombicity, t is the film thickness, h is the length of the twins or the twinning transformation domain size, M is the appropriate shear modulus, σ_c is the stress required to move the film relative to the substrate, and c is a constant approximately equal to unity.[28] Keeping in mind that $\Delta g_{\rm th}$ is negative, i.e., the transformation would like to occur, and that for the transition to occur Δg also must be negative, we see that two quantities, h and t, compete against this: if the relevant domain size of the twinning h and/or the film thickness t is sufficiently small with all else held constant, there will in effect not be enough energy available from the tetragonal-orthorhombic transformation to drive the various processes necessary for the transformation to occur in an unmodified form. The domain size h is dictated by the sample, and thus we can focus our attention on deriving the film thickness below which the transformation will not occur.

To simplify Eq. (1b) on our way to an expression for this minimum thickness, we note that we can minimize the total free energy with respect to twin spacing l and arrive at an expression for the equilibrated twin spacing l_0, as has been done by Welch[28] and by some of the present authors.[29] Doing so gives the equation

$$l_0 = \left[\frac{\gamma}{\sigma_c s/4t + cs^2 M/h} \right]^{1/2} . \tag{2}$$

Now, if we set Δg equal to 0 and substitute our expression for l_0 in for l (thus eliminating it from the equation), and then solve for thickness t, we arrive at an equation for the critical thickness, below which the tetragonal-to-orthorhombic transformation will not occur:

$$t_c^{\rm I} = \sigma_c \left[\frac{(-\Delta g_{\rm th})^2}{s\gamma} - \frac{4csM}{h} \right]^{-1} , \tag{3}$$

where the first term is due to the energy available for the transition and the second term to the energy lost through the grain-size constraint on the twinning.

Similarly, if we postulate that the film consists of unconnected islands as in case II, we may write our free-energy equation as

$$\Delta g = \Delta g_{\rm th} + \Delta g_I' , \tag{4a}$$

where the only terms that have been retained are the free energy of the transformation and the energy required to move the film on the substrate, because an individual island is assumed unconstrained and small enough such that it may transform entirely to a singly oriented domain with a and b axes aligned in only one manner, i.e., no twinning. Working out the energy of deformation for this process yields the specific form

$$\Delta g = \Delta g_{\rm th} + \frac{\sigma_c sd}{4t} , \tag{4b}$$

where all variables are defined as before and d is now the island diameter. Again, the free energy contains a term with an inverse thickness dependence, and the critical thickness becomes

$$t_c^{\rm II} = \frac{\sigma_c sd}{4(-\Delta g_{\rm th})} . \tag{5}$$

The ratio of the two critical thicknesses is then given by

$$\frac{t_c^{\rm I}}{t_c^{\rm II}} = \frac{4\gamma h(-\Delta g_{\rm th})}{(-\Delta g_{\rm th})^2 hd - 4\gamma cds^2 M} \approx \frac{4\gamma}{(-\Delta g_{\rm th})d} , \tag{6}$$

where the approximate equality follows if Δg_m in case I is neglected, i.e., if film-thickness effects dominate.

Although a value for σ_c in the above equations is unavailable and many of the remaining variables are difficult to determine with any certainty (in particular γ and h, which is a moderate function of film thickness and displays a large statistical scatter), the general form of the initial free-energy equation for case I is supported by the approximate $(t)^{1/2}$ thickness dependence of the twin spacing reported by some of us for thin films[29] and by the $(h)^{1/2}$ grain-size dependence observed by others in ceramic material.[34,35] These behaviors are in accordance with the equilibrium twin-spacing formula derived from the free-energy equation and presented in Eq. (2). It therefore seems quite reasonable based on the above analysis to accept the notion of a thermodynamically imposed critical thickness necessary for the tetragonal-to-orthorhombic transition to occur.

Given this critical thickness, it should be noted that the (strained) crystal structure of ultrathin films is very different than the bulk (unstrained) crystal structure. This may have consequences for a variety of other physical properties, including superconductivity. One conceivable way to accommodate this strain is to reduce the amount of oxygen taken up during cooling from the growth temperature. A reduced oxygen content would be consistent with the increased c-axis length observed in ultrathin films[3] and could manifest itself in other measured properties such as a reduced T_c.

C. Implications for multilayer structures

The results from Secs. III A and III B have implications for c-axis-oriented $YBa_2Cu_3O_{7-\delta}$-containing multilayer systems;[7,36–41] also, there should be no reason that the ideas above should not extend to other structures with various rare-earth elements substituted for yttrium, hereafter referred to as RBCO. The growth mechanisms demonstrated above should not be ignored when more complicated structures such as multilayers are deposited.

First, keeping in mind the discrete nuclei of the initial deposit and the unit-cell-ledge growth mechanism observed in our ultrathin films, it is clear that layers will have a roughness due to the ledge steps on the order of one or two full unit cells. The ability of *R*BCO to accommodate strain should aid in the production of continuous layers over the roughness of lower layers. Second, $YBa_2Cu_3O_{7-\delta}$ does not exist in less than a full *c*-axis increment—partial *c*-axis unit cells do not exist. In other words, any deposition sequence of less than a complete unit-cell layer will produce island clusters of fully formed *R*BCO. This has not been explicitly addressed by Triscone *et al.*[36] or by Li *et al.*[37] It is likely that the alloy made by the Geneva group[36] by depositing 0.3 nm of $YBa_2Cu_3O_{7-\delta}$ alternating with 0.3 nm of PrBCO consists of islands of one *R*BCO ringed by the other oxide, which is in turn ringed by the first, and so on, with an appearance much like a bullseye with an annular width on the order of 10 nm. This is not homogeneous with respect to the rare earths as in a solid-solution alloy, but this seems not to affect the macroscopic resistive transition relative to bulk material as the data demonstrate.[36] With regard to the (0.6 nm $YBa_2Cu_3O_{7-\delta}$)/(1.2 nm PrBCO) multilayer of Li *et al.*[37], the microstructure is almost certain to consist of two (50% $YBa_2Cu_3O_{7-\delta}$ islands/50% PrBCO islands) layers and a complete PrBCO layer or, in effect, a large number of unconnected $YBa_2Cu_3O_{7-\delta}$ islands in a PrBCO matrix with poor layering. No good conduction path through the sample exists because of the effective half-area coverage of $YBa_2Cu_3O_{7-\delta}$, and given such a microstructure, it can only be expected that the sample is semiconducting. This is a different microstructure than that implied by the (0.6 nm)/(1.2 nm) notation, and the difference complicates comparison to truly layered structures.

It should be noted that ultrathin $YBa_2Cu_3O_{7-\delta}$ incorporated into a multilayer structure commonly displays a higher T_{c0} and a smaller ΔT_c for a given $YBa_2Cu_3O_{7-\delta}$ layer thickness than the corresponding thickness of bare film. Shorting between superconducting layers has been discounted by one group[37] based on approximately constant sheet conductance with changing PrBCO layer thickness, but shorting is observed by Gupta and coworkers.[38,39] Given the morphology of our ultrathin films, shorting seems likely. It could be that shorts linking a number of $YBa_2Cu_3O_{7-\delta}$ layers in series provides statistically a higher T_c path than in a single-layer ultrathin film. For thicker PrBCO layers, enhanced layer quality as suggested by Li *et al.*, probably in part due to the ease of strain accommodation as seen in Fig. 5(b), is an attractive explanation for the critical temperature differences in ultrathin films and multilayers.

Finally, extending the analysis of Sec. III B to multilayers, it can be seen that if the crystal structure of the other component is not nearly identical to that of the $YBa_2Cu_3O_{7-\delta}$, relative movement at the interfaces is still required for $YBa_2Cu_3O_{7-\delta}$ to transform to its fully orthorhombic state. In some cases this could be an even larger constraint than for ultrathin films because of the greater interfacial area per unit volume involved. Of particular note are the $YBa_2Cu_3O_{7-\delta}$/La-Sr-Cu-O system studied by Eom *et al.*[7] and $YBa_2Cu_3O_{7-\delta}$/Nd-Ce-Cu-O multilayers studied by the IBM Yorktown group.[38,39] Almost no effect is expected in $YBa_2Cu_3O_{7-\delta}$/DyBCO (Ref. 40) because of the very close lattice match. $YBa_2Cu_3O_{7-\delta}$/PrBCO (Refs. 36, 37, and 41) structures should fall somewhere in the middle, given the approximately 1.5% lattice mismatch, of the same order as $SrTiO_3$. As with monolayer ultrathin films, changes in the basic crystal structure from the bulk $YBa_2Cu_3O_{7-\delta}$ case should not be neglected when investigating T_c suppression with decreasing $YBa_2Cu_3O_{7-\delta}$ thickness.

IV. CONCLUSIONS

The microstructures of $YBa_2Cu_3O_{7-\delta}$ ultrathin films have been systematically studied for nomial thicknesses from one unit cell (1.2 nm) to ten unit cells (12 nm). The initial microstructure is found to consist of tetragonal, interconnected, low-aspect-ratio (2.4 nm high by 30 nm diameter) nuclei whose growth is controlled by the propagation in the $YBa_2Cu_3O_{7-\delta}$ *a*-*b* plane of unit-cell-high ledges. The low aspect ratio of the islands gives the deposit a two-dimensional appearance, although growth is not single atomic layer by single atomic layer. TEM dark-field imaging with the $YBa_2Cu_3O_{7-\delta}$ {110} reflection is proposed to be an effective method for exploring the two-dimensional distribution of nuclei thicknesses. With continued deposition these nuclei enlarge laterally such that substrate coverage is increased, followed then by film thickening. By 12 nm the films have completed this initial growth phase, substrate coverage is complete, and the microstructure is the same as in thicker films. A large amount of strain is observed in all of these very thin layers. The mosaic spread of the initial nuclei leads to a high density of threading dislocations, on the order of 10^{11} cm/cm^3, and to an appearance of granularity in the microstructure. By noting a film-thickness dependence of the free energy of the tetragonal-to-orthorhombic transition for a thin film on a rigid substrate, we postulate that motion of the film relative to the film-substrate interface, necessary for the transformation to occur, becomes energetically unfavorable below a certain critical thickness. We advance this as an explanation for the lack of orthorhombic symmetry in ultrathin films. Finally, the observations made for ultrathin films have been applied to $YBa_2Cu_3O_{7-\delta}$ containing multilayers to help describe microstructures encountered in those systems.

Note added in proof. It is of interest to compare the results of this work to those of two recent publications (Hawley, Raistrick, Beery, and Houlton,[42] and Gerber, Anselmetti, Bednorz, Mannhart, and Schlom[47]) concerning the growth of $YBa_2Cu_3O_{7-\delta}$ thin films on $SrTiO_3$ and MgO substrates. Both groups observed a spiral growth morphology in the $YBa_2Cu_3O_{7-\delta}$ film which produced a 1.2-nm-high step for each turn in the spiral (although other step heights were noted). The features observed in our 7.2- and 12-nm-thick films (finite nuclei size, threading edge dislocations at nuclear intersections, and 1.2-nm steps) are all consistent with this spiral growth mecha-

nism, where spiral growth acts quite naturally as the source of the observed steps. For the two thinner films (1.2 and 2.4 nm) where substrate coverage is not complete, the situation is less clear: it is likely that at this stage the requisite spirals are not fully established and other ledge sources must be considered. Finally, in the terminology of this work, and with the findings of (Ref. 42) and (Ref. 43) in mind, growth of these ultrathin films is still considered to be two dimensional, since lateral coverage occurs by attachment onto specific ledge structures. In the thicker films, the continuous production of new terraces via spiral growth—in effect a high nucleation rate for new 1.2-nm-high layers—moves the macroscopic *a-c* growth-rate ratio more toward unity and obscures the two dimensionality of the lateral propagation of the individual layers.

ACKNOWLEDGMENTS

This work has been supported by the Electric Power Research Institute under Contract No. RP8009-11, the Air Force Office for Scientific Research under Contract No. F49620-88-C-004, and by the Stanford Center for Materials Research under the NSF-MRL program. In addition, we would like to thank South Bay Technology, Inc. for the use of the model 515 Dimpler used to prepare microscopy samples for this work. Stimulating interactions with other members of the Stanford high-T_c group and with R. Barton of Conductus, Inc. are gratefully acknowledged. The collaboration of S. Brennan of the Stanford Synchrotron Radiation Laboratory and L. Chyung of Stanford University in acquisition of the GIXS data is appreciated.

[1]M. Grant Norton, Lisa A. Tietz, Scott R. Summerfelt, and C. Barry Carter, Appl. Phys. Lett. **55**, 2348 (1989).

[2]X. X. Xi, J. Geerk, G. Linker, Q. Li, and O. Meyer, Appl. Phys. Lett. **54**, 2367 (1989).

[3]O. Michikami, M. Asahi, and H. Asano, Jpn. J. App. Phys. **29**, L298 (1990).

[4]M. G. Norton and C. B. Carter, Physica C **172**, 47 (1990).

[5]J. Schubert, U. Poppe, and W. Sybertz, J. Less-Common Met. **151**, 277 (1989).

[6]T. Venkatesan, X. D. Wu, B. Dutta, A. Inam, M. S. Hedge, D. M. Hwang, C. C. Chang, L. Nasar, and B. Wilkens, Appl. Phys. Lett. **54**, 581 (1989).

[7]C. B. Eom, S. K. Streiffer, J. Z. Sun, K. Yamamoto, S. S. Laderman, J. C. Bravman, and T. H. Geballe, in *High Temperature Superconductors: Fundamental Properties and Novel Materials Processing,* edited by D. Christen, J. Narayan, and L. Schneemeyer, MRS Symposia Proceedings No. 169 (Materials Research Society, Pittsburgh, 1989, p. 557.

[8]K. Kamigaki, H. Terauchi, T. Terashima, Y. Bando, K. Iijima, K. Yamamoto, and K. Hirata, Physica C **159**, 505 (1989).

[9]T. Terashima, K. Iijima, K. Yamamoto, K. Hirata, Y. Bando, and T. Takada, Jpn. J. Appl. Phys. **28**, L987 (1989).

[10]T. Terashima, Y. Bando, K. Iijima, K. Yamamoto, K. Hirata, K. Kamigaki, and H. Terauchi, Physica C **162-164**, 615, (1989).

[11]J. Gao, B. Häuser, and H. Rogalla, J. Appl. Phys. **67**, 2512 (1990).

[12]Y. Bando, T. Terashima, K. Iijima, K. Yamamoto, K. Hirata, K. Hayashi, K. Kamigaki, and H. Terauchi, in *Proceedings of the XIIth International Congress for Electron Microscopy* edited by L. D. Peachy and D. B. Williams (San Francisco Press, San Francisco, 1990), Vol. 4, p. 2.

[13]C. B. Eom, J. Z. Sun, B. M. Lairson, S. K. Streiffer, A. F. Marshall, K. Yamamoto, S. M. Anlage, J. C. Bravman, T. H. Geballe, S. S. Laderman, R. C. Taber, and R. D. Jacowitz, Physica C **171**, 354 (1990).

[14]For a review of this topic, see W. D. Nix, Metall. Trans. A **20**, 2217 (1989), and references cited therein.

[15]A. L. Roitburd, Phys. Status Solidi A, **37**, 329 (1976).

[16]C. B. Eom, J. Z. Sun, K. Yamamoto, A. F. Marshall, K. E. Luther, and T. H. Geballe, Appl. Phys. Lett. **55**, 595 (1989).

[17]K. Streiffer, C. B. Eom, J. C. Bravman, and T. H. Geballe, in *Proceedings of the XIIth International Congress for Electron Microscopy* (Ref. 12), Vol. 4, p. 6.

[18]U. Dahmen, C. J. D. Hetherington, and K. H. Westmacott, in *Proceedings of the XIIth International Congress for Electron Microscopy* (Ref. 12), Vol. 4, p. 338.

[19]C. J. D. Hetherington, in *High Resolution Electron Microscopy of Defects in Materials,* edited by R. Sinclair, D. Smith, and U. Dahmen, MRS Symposia Proceedings No. 183 (Materials Research Society, Pittsburgh, 1990), p. 123.

[20]MacTempas HREM Image Simulation Software, copyright Total Resolution, Berkeley, CA.

[21]D. G. Schlom, Ph.D. dissertation, Standford University, 1990.

[22]S. K. Streiffer, B. M. Lairson, C. B. Eom, A. F. Marshall, J. C. Bravman, and T. H. Geballe, in *High Resolution Electron Microscopy of Defects in Materials* (Ref. 19), p. 363.

[23]G. E. Dieter, *Mechanical Metallurgy* (McGraw-Hill, New York, 1986), p. 230.

[24]D. M. Hwang, T. S. Ravi, R. Ramesh, Siu-Wai Chan, C. Y. Chen, L. Nazar, X. D. Wu, A. Inam, and T. Venkatesan, Appl. Phys. Lett. **57**, 1690 (1990).

[25]D. M. Hwang, T. Venkatesan, C. C. Chang, L. Nazar, X. D. Wu, A. Inam, and M. S. Hedge, Appl. Phys. Lett. **54**, 1702 (1989).

[26]Ch. Leemann, Ph. Flückiger, V. Marsico, J. L. Gavilano, P. K. Srivastava, Ph. Lerch, and P. Martinoli, Phys. Rev. Lett. **64**, 3082 (1990).

[27]G. Arlt, D. Hennings, and G. de With, J. Appl. Phys. **58**, 1619 (1985).

[28]D. O. Welch (unpublished results) as referred to in Yowen Xu, M. Suenaga, J. Tafto, R. L. Sabatini, and A. R. Moodenbaugh, Phys. Rev. B **39**, 6667 (1989).

[29]B. M. Lairson, S. K. Streiffer, and J. C. Bravman, Phys. Rev. B **42**, 10 067 (1990).

[30]J. D. Budai, R. Feenstra, and L. A. Boatner, Phys. Rev. B **39**, 12 355 (1989).

[31]S. K. Streiffer and J. C. Bravman (unpublished).

[32]J. C. Barry, J. Electron Microsc. Tech. **8**, 325 (1988).

[33]H. Schmid, E. Burkhardt, E. Walker, W. Brixel, M. Clin, J.-P. Rivera, J.-L. Jorda, M. François, and K. Yvon, Z. Phys. B **72**, 305 (1988).

[34]T. M. Shaw, S. L. Shinde, D. Dimos, R. F. Cook, P. R. Duncombe, and C. Kroll, J. Mater. Res. **4**, 248 (1989).
[35]L. S. Chumbley, J. D. Verhoven, M. R. Kim, A. L. Corneliu, and M. J. Kramer, IEEE Trans. Magn. **MAG-25**, 2337 (1989).
[36]J.-M. Triscone, Ø. Fischer, O. Brunner, L. Antognazza, A. D. Kent, and M. G. Karkut, Phys. Rev. Lett. **64**, 804 (1990).
[37]Q. Li, X. X. Xi, X. D. Wu, A. Inam, S. Vadlamannati, W. L. McLean, T. Venkatesan, R. Ramesh, D. M. Hwang, J. A. Martinez, and L. Nazar, Phys. Rev. Lett. **64**, 3086 (1990).
[38]A. Gupta, R. Gross, E. Olsson, A. Segmüller, G. Koren, and C. C. Tsuei, Phys. Rev. Lett. **64**, 3191 (1990).
[39]R. Gross, A. Gupta, E. Olsson, A. Segmüller, and G. Koren, Appl. Phys. Lett. **57**, 203 (1990).
[40]J.-M. Triscone, M. G. Karkut, L. Antognazza, O. Brunner, and Ø. Fischer, Phys. Rev. Lett. **63**, 1016 (1989).
[41]Douglas H. Lowndes, David P. Norton, and J. D. Budai, Phys. Rev. Lett. **65**, 1160 (1990).
[42]Marilyn Hawley, Ian D. Raistrick, Jerome G. Beery, and Robert J. Houlton, Science **251**, 1587 (1991).
[43]C. Gerber, D. Anselmetti, J. G. Bednorz, J. Mannhart, and D. G. Schlom, Nature **350**, 279 (1991).

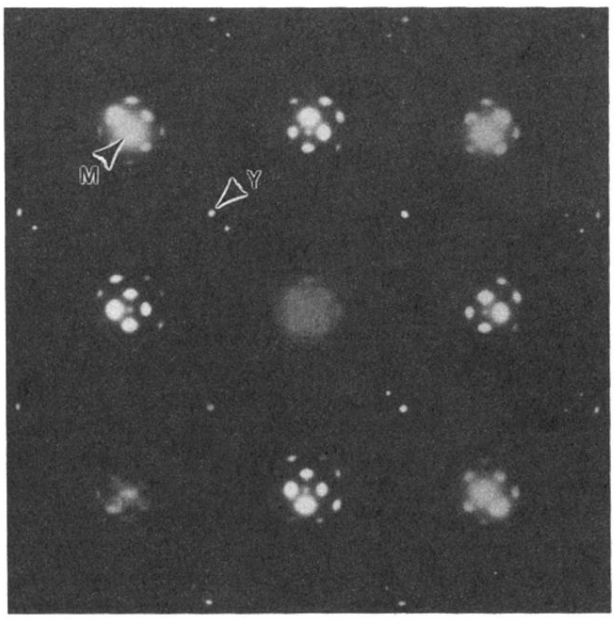

FIG. 1. Plan-view electron-diffraction pattern of 2.4-nm-thick $YBa_2Cu_3O_{7-\delta}$ film on MgO. The $YBa_2Cu_3O_{7-\delta}$ (100) spot is indicated by Y and the MgO (200) by M for reference. The spot intensities in this pattern have been substantially altered such that the $YBa_2Cu_3O_{7-\delta}$ spots are visible on the final photograph.

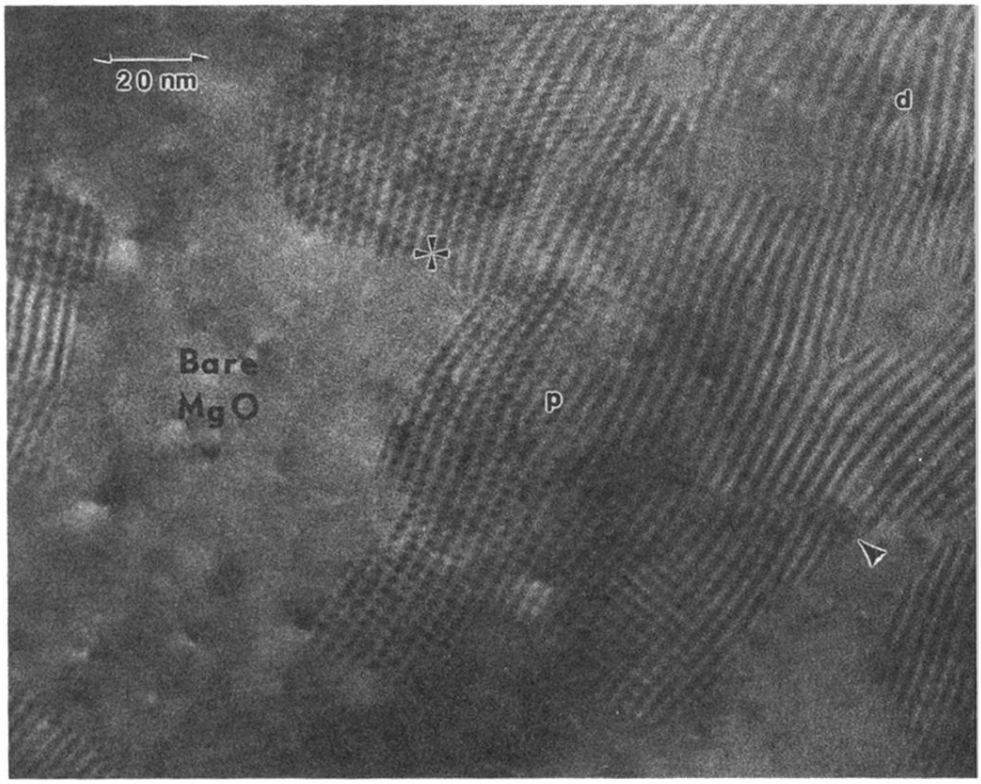

FIG. 2. Plan-view image of 1.2-nm-thick film showing moiré fringes arising from spacing difference of $YBa_2Cu_3O_{7-\delta}$ and MgO (200)'s. Fringe spacing is approximately 2.3 nm. Dark and light background mottling is due to electron-beam-induced damage in the MgO substrate. A variety of defects are present, including full dislocations, example marked *d*, partial dislocations, example marked *p*, and a translation boundary, marked by the arrow. Also present are abrupt integrated image intensity changes due to discrete thickness changes in the film. The end of one such boundary is marked by a star.

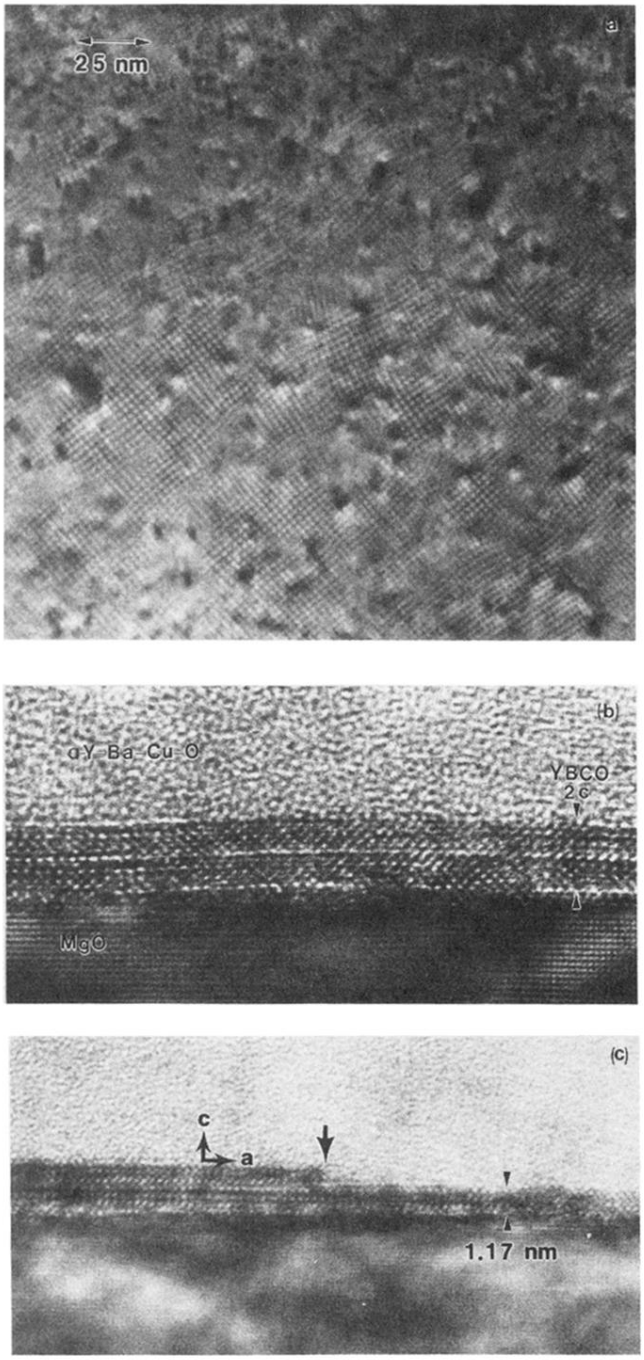

FIG. 4. (a) Plan-view image of 2.4-nm film. Note increased substrate coverage over 1.2-nm film. (b) Cross section of 2.4-nm film. Visible are the MgO, the two-unit-cell-thick $YBa_2Cu_3O_{7-\delta}$ film, and the amorphous $YBa_2Cu_3O_{7-\delta}$ (α-Y-Ba-Cu-O) overlayer. Note the frequent curving of the lattice planes in the $YBa_2Cu_3O_{7-\delta}$ film. (c) Cross section showing unit-cell-high ledge, marked by large arrow. The $YBa_2Cu_3O_{7-\delta}$ crystallographic directions are as indicated.

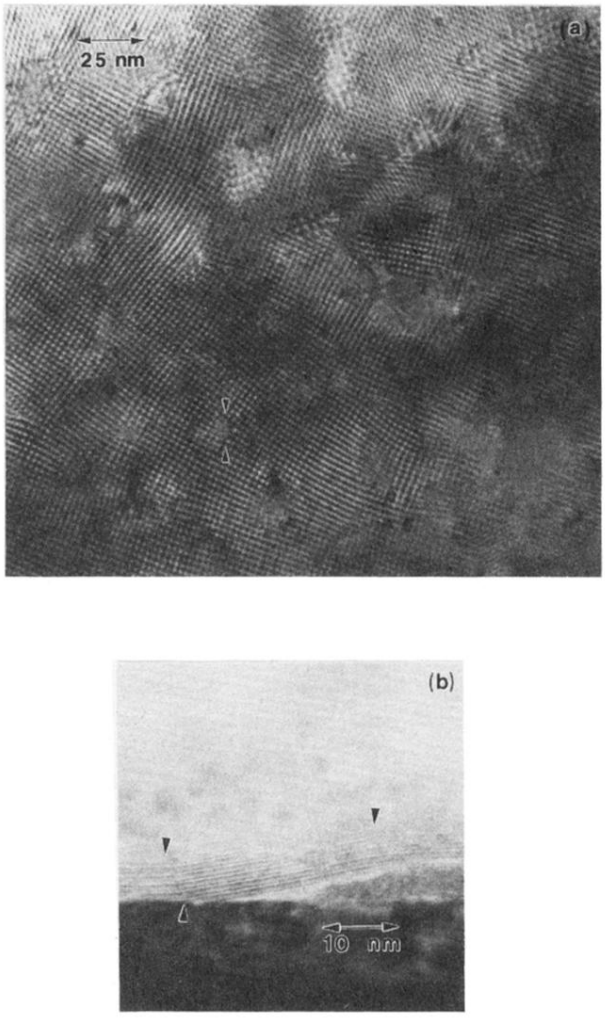

FIG. 5. (a) Plan-view micrograph of the 7.2-nm film. At this stage coverage is nearly complete. The threading dislocation density measured from this image is 10^{11} cm/cm^3. A representative dislocation lies between the arrows; viewing is best performed by sighting down the moiré fringes. (b) Cross section of 7.2-nm film. The film has grown over a substrate surface perturbation, with the strain partly accommodated by low-angle boundaries, marked by arrows. There is some ion-mill damage of the film in this region, increasing toward the right of the image.

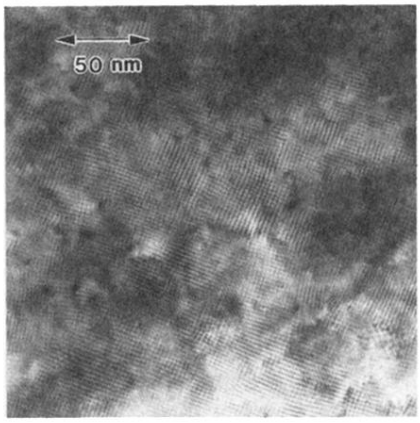

FIG. 6. Plan-view image of the 12-nm film.